Chinese Journal of Chemical Engineering 47 (2022) 271–281

Contents lists available at ScienceDirect

Chinese Journal of Chemical Engineering

journal homepage: www.elsevier.com/locate/CJChE

Full Length Article

The study of the effect of gas-phase fluctuation on slag flow and refractory brick corrosion in the slag tapping hole of an entrained-flow gasifier

Kuo Lin, Zhongjie Shen, Qinfeng Liang, Jianliang Xu *, Haifeng Liu *

Shanghai Engineering Research Center of Coal Gasification, East China University of Science and Technology, Shanghai 200237, China
Institute of Clean Coal Technology, East China University of Science and Technology, Shanghai 200237, China

ARTICLE INFO

Article history:
Received 1 April 2021
Received in revised form 17 July 2021
Accepted 18 July 2021
Available online 30 August 2021

Keywords:
Gasification
Brick corrosion
Dynamic response
Slag flow
Heat transfer

ABSTRACT

The service life of refractory brick in the slag tapping hole of the entrained flow gasifier was significantly lower than that in other locations. It was critically important to study the corrosion mechanism of refractory brick in the slag tapping hole for guiding industrial production. Considering the complex flow field in the slag tapping hole, the influence of gas velocity and temperature fluctuation on the service life of refractory brick was investigated in this study. The results showed that the slag flow characteristics periodically changed with the gas temperature and velocity fluctuations. The brick corrosion rate increased with the decrease of fluctuation frequency. Compared with the gas-phase velocity fluctuation, the gas-phase temperature fluctuation had a more significant influence on the brick corrosion rate. When the fluctuation frequency was 0.01 Hz and the gas temperature fluctuation amplitude was 200 K, the corrosion rate of refractory bricks increased by 25%. It could be concluded that the fluctuation of gas-phase temperature was the main cause for the low service life of refractory bricks in the tapping hole.
© 2021 The Chemical Industry and Engineering Society of China, and Chemical Industry Press Co., Ltd. All rights reserved.

1. Introduction

The coal production and consumption in China increased by 3.2 EJ and 1.8 EJ in 2019, respectively [1]. Benefited from abundant reserves, coal became an important part of Chinese energy consumption structure [2]. With the increasing knowledge of emission reduction, coal gasification technology which used coal resources in a clean and efficient way became the pillar industry of the coal chemical industry [3,4].

At present, entrained-flow gasification was widely used, which could be classified into two types: membrane wall lining gasifiers and refractory brick lining gasifiers [5,6]. Due to its excellent thermal insulation performance, the refractory brick lining gasifier had a small radial heat flux and a high conversion efficiency [7]. Correspondingly, the surface temperature of the refractory brick wall was higher than the temperature of slag critical viscosity, therefore there was no solid slag layer on the refractory brick [8]. Due to the lack of protection of the solid slag layer, the service life of the refractory layer of the refractory brick lining gasifier was shorter than that of the membrane wall lining gasifier. Besides, the service life of refractory bricks in different areas was significantly different even for a gasifier. The brick service life of the slag tapping hole was approximately 1/2 times of that of the straight section in the commercial gasifiers [9]. The huge difference in refractory brick service life in different areas greatly affected the use efficiency of refractory brick and the operation period of the gasifier.

Many efforts have been made to study the corrosion process of the refractory brick [10–13]. Kaneko *et al.* [14] studied the infiltrations of synthetic coal slag into 99% Al_2O_3, 85% Al_2O_3-15% SiO_2, and 90% Cr_2O_3-10% Al_2O_3 refractories, and found that the corrosion resistance of different refractory materials varied greatly. Andrés *et al.* [15] made laboratory static and dynamic tests to evaluate the decomposition process of refractory brick, and found that the alumina-magnesia-carbon refractory bricks exhibited similar corrosion mechanisms in both the static and dynamic tests. Zhao *et al.* [16] built a thermodynamics model to study the loss process of refractory brick and found that the slag penetration could aggravate the corrosion of refractory bricks. The slag flow characteristics also played an important role in the corrosion process of the refrac-

* Corresponding authors at: Shanghai Engineering Research Center of Coal Gasification, East China University of Science and Technology, P.O. Box 272, Shanghai 200237, China. Fax: +86 21 64251312.
E-mail addresses: xujl@ecust.edu.cn (J. Xu), hfliu@ecust.edu.cn (H. Liu).

https://doi.org/10.1016/j.cjche.2021.07.029
1004-9541/© 2021 The Chemical Industry and Engineering Society of China, and Chemical Industry Press Co., Ltd. All rights reserved.

tory brick. At present, numerous simulation methods about the slag flow characteristics were concentrated on the particle deposition mechanism and the modeling of the slag flow process [17,18]. Considering the near-wall phenomena of char particles transferring from the furnace to the wall, Troiano *et al.* [19] built a compartmental model of entrained-flow slagging gasifiers. The submodel of particle deposition showed high accuracy. Ye *et al.* [20] built a steady-state model to study the slag flow process. When the temperatures of the solid slag layer and reactor wall were determined, the new control volumes would be added onto the existing slag surface accompanied by the particles deposition. Lee *et al.* [21] built a comprehensive dynamic model to simulate the slag flow and heat transfer process of the Shell gasifier. The results showed that when the operating conditions changed, the system would be stable in approximately 500 s. Based on the analysis of mass, energy and momentum of the slag flow process, Seggiani [22] proposed a classic model which could be used to simulate the dynamic response process of slag in a Prenflo entrained-flow gasifier. These models were proved to be of great advantage and reliability to study the slag flow characteristics.

However, the present studies could not reveal the relationship between the low service life of refractory bricks and the slag flow process. It should be pointed out that the corrosion rate of refractory brick in the slag tapping hole was 2–3 times of that in the straight section for the commercial gasifier. In our previous research [23,24], it was found that the external diffusion model could be used to predict the corrosion rate of refractory bricks in the dome portion and straight portion for a top single-burner down-flow gasifier (whose structure was shown in Fig. 1). For the lower cone and slag tapping hole, the brick corrosion rate was higher than that in the straight portion, but it was still lower than industry data. Some references [25] proposed that the temperature fluctuation amplitude increased along the jet direction in the jet field. Namely, the gas-flow fluctuation of the slag tapping hole was inherently stronger than that in the straight portion. Besides, considering the complex flow field caused by the sudden reduction of the diameter of the slag tapping hole, the gas-phase fluctuation was significantly severe. Therefore, in order to investigate the corrosion mechanism of refractory brick in the slag tapping hole, the effects of gas-phase fluctuation on the corrosion process of refractory brick were studied in this work.

2. Model Description

2.1. The slag flow and heat transfer model

The lower cone and slag tapping hole of a single-burner water-slurry entrained-flow gasifier structure was selected as the research object, whose structure was shown in Fig. 1. Because the studied area was located at the bottom of the gasifier, fewer residual carbon particles existed. Therefore, the heat evolution resulting from the slag evaporation was neglected in the slag flow and heat transfer process to simplify the modeling process. The numerical simulation method proposed by Seggiani [22] and Zhang *et al.* [26] was used to simulate the slag flow process in the refractory brick lining gasifier. The purpose of this work was to study the effect of gas-phase fluctuation in the furnace on the corrosion process of refractory brick. Therefore, in this work described here, a brief numerical methodology was described. And the detailed modeling method could be found in our previous work [7,23,24,27].

The viscosity and velocity of molten slag on the wall were approximately 3–20 Pa·s and 0.5–20 cm·s^{-1}, respectively [28]. Therefore, the slag was a laminar flow on the refractory wall [29]. The slag was dispersed into a series of control volumes along the axial direction. In each control volume, the mass, momentum and energy of slag were conserved (Eqs. (1)–(3)). The slag velocity (Eq. (4)) could be obtained by the double integration of the momentum equation.

$$\frac{\mathrm{d}}{\mathrm{d}x}\left(\eta_s \frac{\mathrm{d}u_i}{\mathrm{d}x}\right) = -\rho_s g \cos\beta \tag{1}$$

where $x = 0, \eta_s \dfrac{\mathrm{d}u_i}{\mathrm{d}x} = \tau$ and $x = \delta_s,\ u_i = 0$.

$$\rho A_1 \frac{\mathrm{d}\delta_s}{\mathrm{d}t} = m_{in} + m_{ex,i-1} - m_{ex,i} \tag{2}$$

$$\rho_s c_s A_1 \frac{\mathrm{d}(\delta_s T_s)}{\mathrm{d}t} = Q_{in} + Q_{ex,i-1} - Q_{ex,i} - Q_{sr1,i} \tag{3}$$

$$u(x) = \frac{\rho g \cos\beta\left(\delta_s^2 - x^2\right)}{2\eta_s} + \frac{\tau(\delta_s - x)}{\eta_s} \tag{4}$$

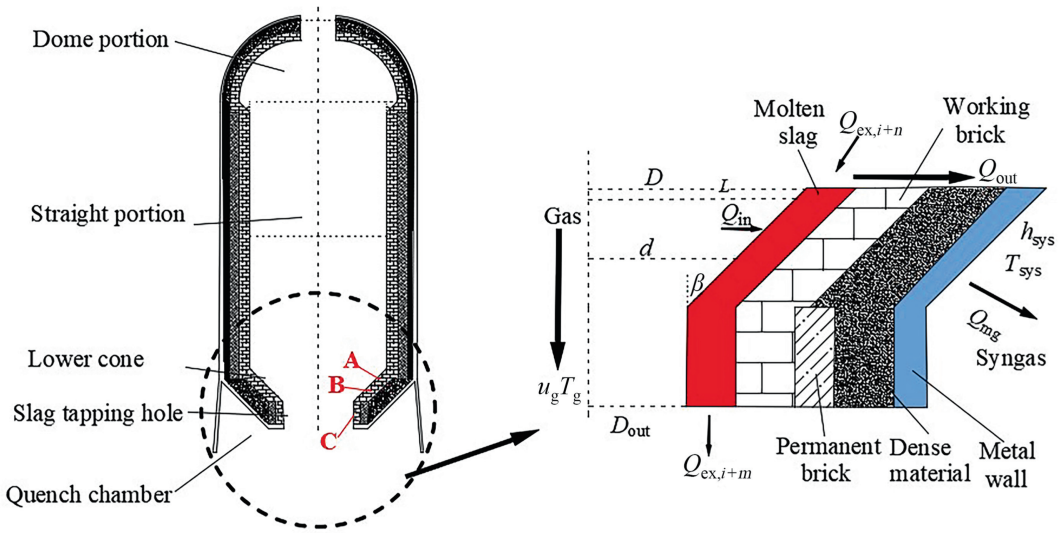

Fig. 1. Schematic diagram of the gasifier.

In the momentum conservation equation, the item τ was the shear force exerted by the gas-flow in the furnace, which was estimated by: $\tau = C\rho_g u_g^2$ (where C was model parameter and was equal to 0.0303) [24]. The average thermal conductivity between slag and brick in the process of heat transfer could be expressed by the following equation:

$$\frac{\bar{\delta}}{\bar{\lambda}} = \frac{\delta_s}{\lambda_s} + \frac{\delta_{r1}}{\lambda_{r1}} \rightarrow \bar{\lambda} = \frac{(\delta_s + \delta_{r1})\lambda_s\lambda_{r1}}{\delta_s\lambda_{r1} + \lambda_s\delta_{r1}} \tag{5}$$

2.2. The model of gas temperature fluctuation

In the commercial gasifier, coal gasification involved multiple physics processes, such as turbulence, chemistry, particle transport, *etc*. Compared with the straight portion, the gas-phase velocity inside the slag tapping hole was higher. The local temperature was critically dependent on the ambient flame conditions. Due to the turbulent flow field coupled with the violent gasification reaction, the temperature and velocity of the gas phase periodically fluctuated within a certain range [30]. Gong *et al.* [31] studied the flame characteristics in an opposed multi-burner gasifier, and found that the fluctuation frequencies of the flame were concentrated in the low-frequency region. Tsue *et al.* [25] studied the temperature and velocity fluctuation of a jet diffusion flame in a cross-flow. It could be concluded that the temperature fluctuation and velocity fluctuation showed an increase and decrease along the jet direction in the jet field, respectively. Xing *et al.* [32] studied the coal devolatilization characteristics with gas temperature fluctuation, and found that the turbulent flow field with gas temperature fluctuation was controlled by the turbulence, chemistry, particle transport, heat and mass transfer. Shaw *et al.* [30] monitored the temperature evolution in pulverized coal flames by the data evaluation of the two-color signal, and found that the fluctuations in concentration and size distribution contributed to the flame fluctuation. Xia *et al.* [33] proposed a vortex-dynamical scaling theory for flickering buoyant diffusion flames. In the present work, Xia' model [33] and Shaw' method [30] were used to describe the gas temperature fluctuation process, and the gas temperature fluctuation amplitudes and flame fluctuation frequency could be expressed as follows:

$$R' = (K_1/K_2)\left(\varepsilon_{\lambda_1}/\varepsilon_{\lambda_2}\right)(\Delta\lambda_1/\Delta\lambda_2)(\lambda_2/\lambda_1)^5 \exp\left(c(1/\lambda_1 - 1/\lambda_2)/T_g\right) \tag{6}$$

$$T_g = \left(\frac{c}{\lambda_1} - \frac{c}{\lambda_2}\right)/\ln(aR') \tag{7}$$

$$f = \sqrt{\frac{C_h(r^* - 1)}{2C_D}} \cdot \frac{g}{D} \tag{8}$$

The fluctuation frequency was proportional to the $\sqrt{g/D}$. In the studied gasifier, $\sqrt{g/D} = 2.4$ (D was the gasifier diameter).

2.3. The refractory brick corrosion model

The corrosion of refractory brick was a complex process, which was controlled by many factors, such as the operating conditions, the mineral composition of slag, the thermal shock, and the brick types, *etc*. [34–36]. At present, the chrome oxide was usually used as the working brick due to its high corrosion resistance to slag in high temperature and pressure conditions in commercial gasifiers [37]. In our previous work [23,24], based on the mechanism of liquid–solid diffusion, the external diffusion model was built to study the refractory brick corrosion process. It was found that the external diffusion model could accurately predict the corrosion rate of refractory bricks in the straight portion of the entrained-flow gasifier. The brick corrosion rate in the external diffusion model could be expressed by the following equation:

$$J = C_f \frac{T_s^{2/3} u_s^{1/2}}{\eta_s^{1/6}\delta_s^{1/2}} = C_f' \frac{T_s^{2/3} m_{ex}^{1/2}}{\eta_s^{1/6}\delta_s} \tag{9}$$

where C_f was a parameter in the brick corrosion model and equal to 3.55×10^{-3} [23].

Table 1
Slag compositions and properties

Slag compositions Component/% (mass)		Slag properties	Value
SiO_2	42.44	Critical viscosity temperature/K	1400
Al_2O_3	18.87	Density/kg·m^{-3}	2535
CaO	14.76	Thermal conductivity/W·m^{-1}·K^{-1}	1.43
Fe_2O_3	8.51	Specific heat/J·kg^{-1}·K^{-1}	1670
SO_3	9.48		
MgO	1.09		
Na_2O	2.50		
K_2O	0.71		
TiO_2	1.01		
Others	0.63		

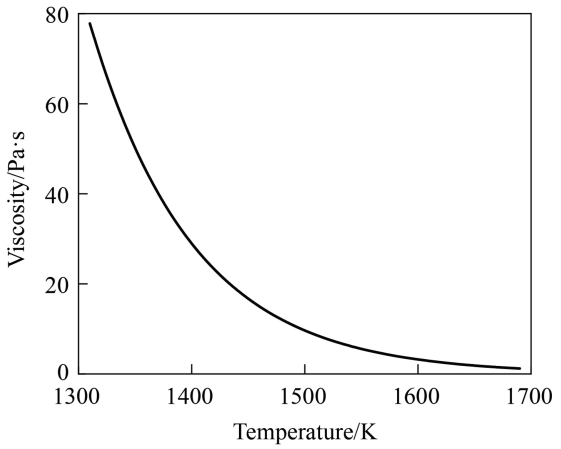

Fig. 2. Viscosity-temperature characteristics of coal slag.

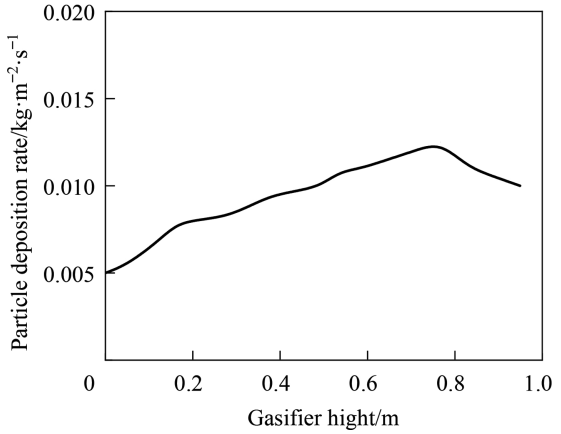

Fig. 3. Particle deposition rate along the wall.

3. Simulation Conditions and Methods

A commercial-scale gasifier fed with 1500 tons of coal was selected as the object in this study. The slag temperature-viscosity characteristics and the slag composition were determined using a high temperature rotational viscometer (Theta Industries, Port Wash, NY, USA), and a X-ray fluorescence analyzer (Thermo Scientific, USA), as shown in Table 1 and Fig. 2. According to Xu *et al.*'s method [38], the numerical simulation of the gas-phase field was built. The steady-state Reynolds-averaged Navier-Stokes equations and the realizable k-ε model were adopted to describe the gas-phase turbulent flow. The eddy dissipative concept model was used to model homogeneous reactions. The random trajectory model and standard wall function were used to track each particle.

Table 2
Model parameters

Structure parameters	Value
D/mm	1852–3352
δ_{r1}/mm, λ_{r1}/W·m^{-1}·K^{-1}, ρ_{r1}/kg·m^{-3}	360, 4.0, 4300
δ_{r2}/mm, λ_{r2}/W·m^{-1}·K^{-1}, ρ_{r2}/kg·m^{-3}	300, 0.9, 3300
δ_{m}/mm, λ_{m}/W·m^{-1}·K^{-1}, ρ_{m}/kg·m^{-3}	100, 17, 7800
Boundary conditions	**Value**
ε_{θ}	0.83 [22]
σ/W·m^{-2}·K^{-4}	5.67×10^{-8}
h_{sys}/W·m^{-2}·K^{-1}	96 [38]
T_{sys}/K	515 [38]
L/m	0.03

And the further modeling method could be found in Ref [38]. Based on the numerical simulation of the gas-phase field, the particle deposition rate was obtained, as shown in Fig. 3.

With the deposition rate as the input parameter, the slag flow and heat transfer model could be solved, whose model parameters were listed in Table 2. To study the influence of the gas-flow fluctuation on brick corrosion rate, the unity of the variable was necessary. And the other parameters should remain unchanged except for the gas-flow temperature and velocity fluctuation. Therefore, a certain position inside the tapping hole (0.438 m from the top of the lower cone) was selected as the object in this work, where slag mass flow rate was equal to the mean values of the whole hole. The generally used brick type in the commercial gasifier, chromia-alumina–zirconia refractory, was adopted as the working brick in this study, whose chemical composition was 86% Cr_2O_3-7% ZrO_2 and apparent Porosity was 17%. The thickness of working brick, dense castable refractory was 0.36 m and 0.3 m, respectively. The thermal conductivity and specific heat of slag were constants independent of temperature.

The equations of slag flow and heat transfer were the coupled non-linear systems, which were solved with the help of Matlab software. There were some ODE (ordinary differential equation) solvers in Matlab which could be used to solve differential equations. The stiff equations solving method, Gear's method (ODE15s) was adopted. The definite integral equations were solved by Simpson's 1/3 rule of integration. The outputs of the slag flow and heat transfer model including the slag temperature, slag velocity, slag thickness were the input parameters of the brick corrosion model. The integration of different models could be expressed as in Fig. 4.

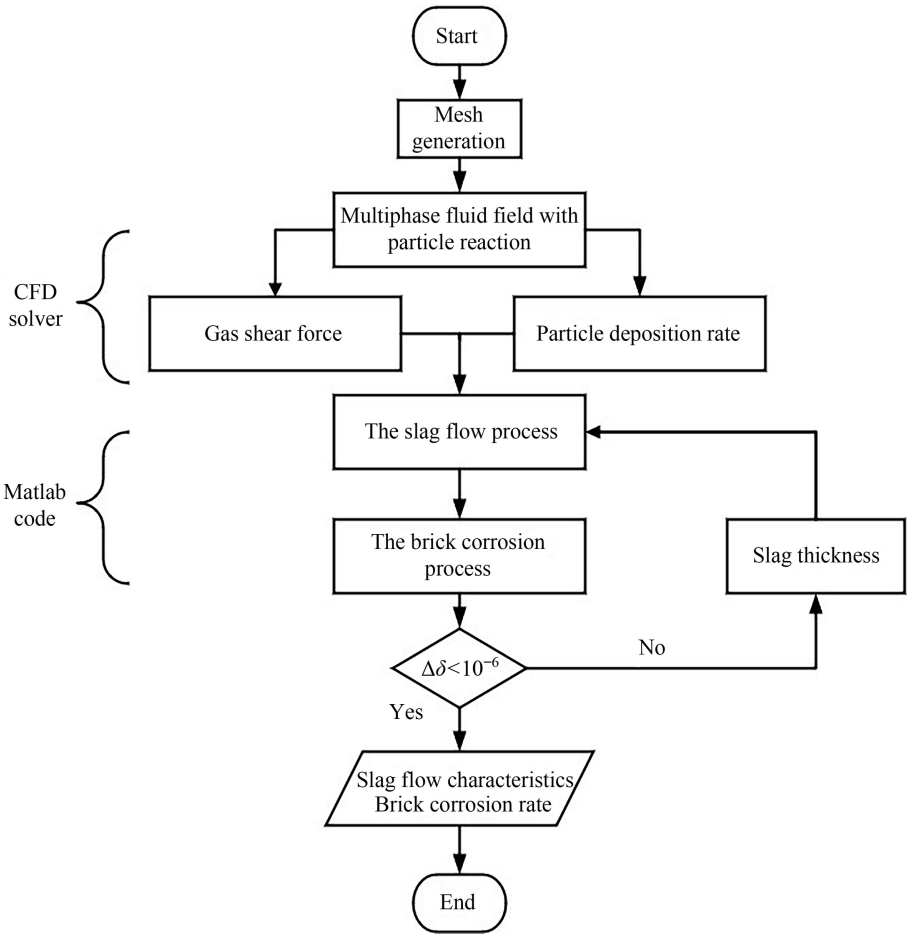

Fig. 4. Calculation flowchart of the main program.

4. Results and Discussion

4.1. Steady state

In order to evaluate the interaction between operating conditions and slag flow behavior, the slag flow characteristics with different operating temperatures under steady-state conditions were studied, as shown in Fig. 5. The operating temperature of the refractory brick lining gasifier was usually 1450–1650 K. To study the influence of operating temperature, a more wide range of operating temperature (1500–1800K) was adopted. As the operating temperature increased, the radial heat flux increased. The heat transferred from the gas to the slag increased, resulting in the increase of the slag temperature and the decrease of slag viscosity. The gas temperature and wall thermal resistance which was mainly composed of the slag layer and refractory brick layer determined the slag temperature. Because the thickness of the slag layer was much less than that of the refractory layer, the change of heat resistance was significantly slight with the change of operating temperature. Therefore, the increase of the slag temperature was linear with the increase of the gas temperature, and the slag temperature was almost equal to the gas temperature under steady-state conditions. The evolution of slag viscosity directly affected the thickness and flow velocity of the slag. As the gas-phase temperature increased from 1500 K to 1800 K, the thickness of the slag decreased from 4.38 mm to 1.49 mm, and the slag flow velocity increased from 1.86 cm·s^{-1} to 5.62 cm·s^{-1}.

In steady-state conditions, the distribution of refractory brick corrosion rate of the slag tapping hole with different operating temperatures is shown in Fig. 6. The corrosion rate of refractory bricks increased exponentially with the increase of operating temperature. When the operating temperature increased from 1500 K to 1800 K, the brick corrosion rate increased by 3.179 mm·100 h^{-1} (504.76%), which demonstrated that the change of gas mean temperature was the key factor for the corrosion of refractory bricks.

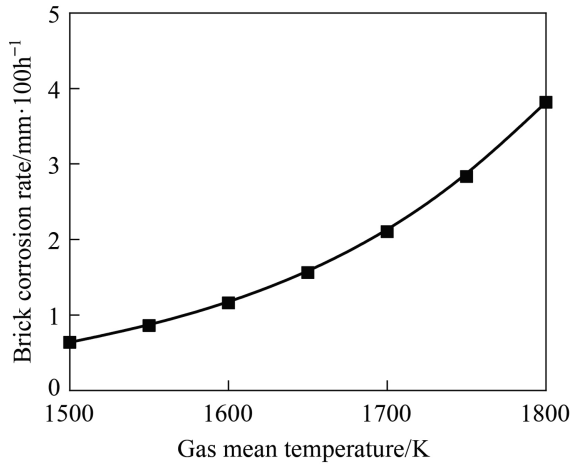

Fig. 6. The influence of the gas mean temperature on the brick corrosion rate.

4.2. Dynamic state

The temperature and velocity of the gas phase in the gasifier were not the constants due to the turbulent flow field coupled with the violent gasification reaction. The velocity and temperature of the gas phase fluctuated within a certain range [39]. Therefore, in this section, the effects of gas-phase fluctuation frequency, velocity fluctuation and temperature fluctuation on the slag flow characteristics and the corrosion process of the refractory bricks were studied, respectively.

4.2.1. Gas fluctuation frequency

In the gasifier, the gas temperature fluctuated around the average temperature and exhibited periodic behavior [30]. To ensure the unity of the variable, it was necessary to ensure that other parameters remain unchanged except for the operating temperature. Therefore, it was assumed that the gas temperature changed sinusoidally and other operating conditions remained unchanged in this section. The gas temperature could be expressed as follows:

$$T_g = \bar{T}_g + T'_g \sin(2\pi f t) \quad (10)$$

In this section, the gas mean velocity was 9 m·s^{-1}, the gas mean temperature and the temperature fluctuation amplitude were assumed to be 1600 K and 150 K, respectively. Figs. 7 and 8 show the effects of gas fluctuation frequencies on slag flow characteristics. The results showed that the slag flow characteristics changed approximately sinusoidal with temperature fluctuations. And the fluctuation amplitude of the slag temperature and velocity gradually increased as the gas temperature frequency decreased, which demonstrated that the effects of low-frequency fluctuation on slag flow were greater than that of high-frequency fluctuation. Besides, the slag temperature was more sensitive to the evolution of the gas phase temperature than the slag velocity. When the fluctuation frequencies were 0.01 Hz and 0.1 Hz, the fluctuation amplitudes of the slag temperature were basically the same, only the fluctuation periods were different. However, the fluctuation amplitude of slag velocity decreased with the increase of the fluctuation frequency. When the gas fluctuation frequencies were 0.01 Hz, 0.1 Hz and 1 Hz, the fluctuation amplitudes of slag velocity were 4.05 cm·s^{-1}, 0.83 cm·s^{-1} and 0.07 cm·s^{-1}, respectively.

The influence of fluctuation frequency on the brick corrosion rate is shown in Fig. 9. When there was no fluctuation in the gas phase, the corrosion rate of refractory brick was 1.170 mm·100 h^{-1}. With the change from high-frequency fluctuation to low-frequency

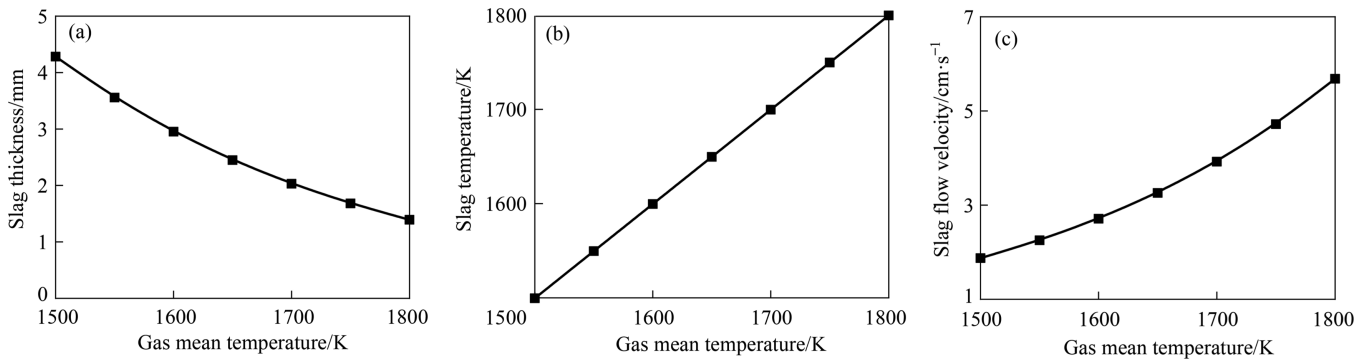

Fig. 5. The influences of the gas mean temperature on (a) slag thickness, (b) slag temperature and (c) slag velocity.

fluctuation, the effect of gas temperature on the corrosion rate of refractory brick became significant, which was consistent with the effect of frequency on slag flow characteristics. Therefore, in order to improve the service life of the refractory brick, the low-frequency fluctuation of temperature should be avoided by adjusting the oxygen coal ratio in the commercial gasifier.

In order to study the influence mechanism of fluctuation frequency on slag temperature, the response process of the slag temperature to the gas temperature transient change was studied, as shown in Fig. 10. When the gas temperature increased suddenly from 1600 K to 1750 K, the heat transferred from the gas phase to the slag layer increased. However, due to the hysteresis of the thermal transfer process, the response time of the slag temperature was about 5 s. Therefore, the characteristic fluctuation frequency of slag temperature was approximately 0.2 Hz. With the increase of frequency, the fluctuation period decreased. When it was less than the characteristic response time of slag, the change of gas-phase temperature could not be completely transferred to the slag layer. Therefore, the fluctuation amplitude of slag temperature gradually decreased with the increase of the fluctuation frequency.

4.2.2. Gas velocity fluctuation amplitude

In this section, the influence of gas-phase velocity fluctuation was investigated. Assuming that the gas-phase velocity was a reg-

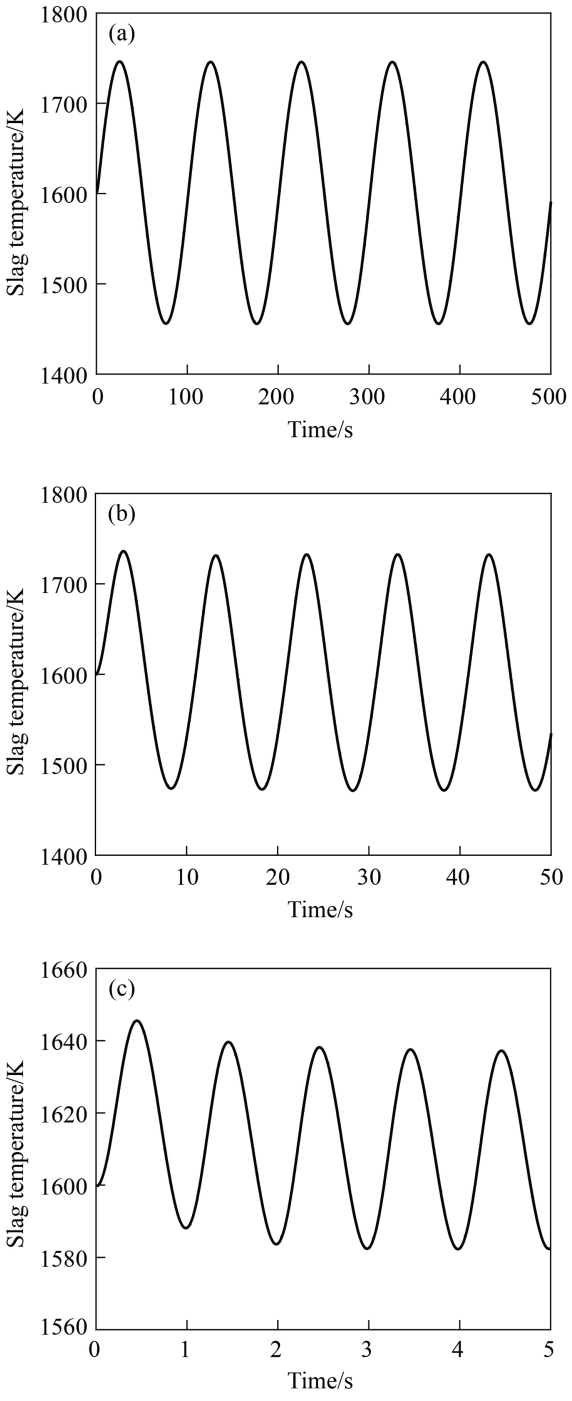

Fig. 7. The influences of the gas fluctuation frequency on the slag temperature: (a) f = 0.01 Hz, (b) f = 0.1 Hz and (c) f = 1 Hz.

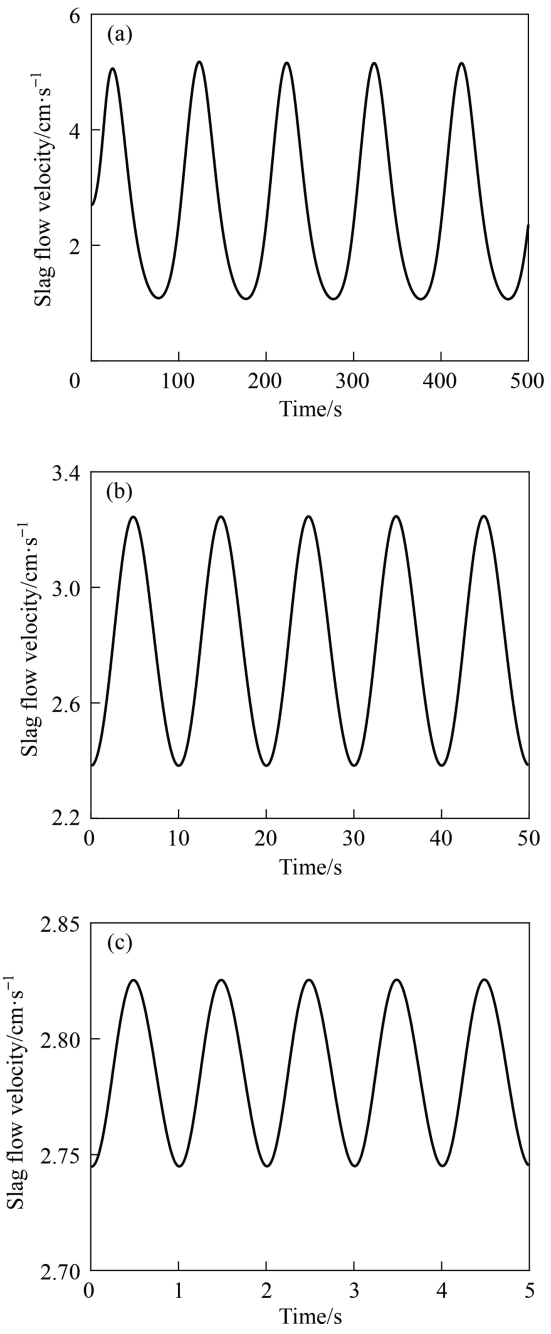

Fig. 8. The influences of the gas fluctuation frequency on the slag velocity: (a) f = 0.01 Hz, (b) f = 0.1 Hz and (c) f = 1 Hz.

ular sinusoidal distribution, the gas phase velocity could be expressed by Eq. (11).

$$u_g = \bar{u_g} + u'_g \sin(2\pi f t) \tag{11}$$

The gas mean temperature and velocity were 1600 K, and 9 $m \cdot s^{-1}$, respectively. The influence of gas velocity fluctuation amplitude on the slag flow characteristics is shown in Fig. 11. Under the condition of constant fluctuation frequency (f = 0.1 Hz), the larger the velocity fluctuation amplitudes were, the greater the effects on slag flow process were. Besides, the responses of different characteristic parameters to gas velocity fluctuations were different. Because the slag thickness was much smaller than that of refractory brick, the change of slag thickness caused by gas velocity fluctuation had little effect on the total radial thermal resistance, resulting in the slight amplitude of slag temperature, as shown in Fig. 11 (b). When the fluctuation amplitude of gas-phase velocity was 4 $m \cdot s^{-1}$, the slag temperature fluctuation amplitude was only 0.02 K. Correspondingly, the highest changing amplitude of slag thickness and velocity were 0.37 mm and 1.05 $mm \cdot s^{-1}$, respectively.

Fig. 12 shows the effect of gas-phase velocity fluctuation on the corrosion rate of refractory bricks. With the increase of velocity fluctuation amplitude, the corrosion rate of the refractory bricks gradually increased. However, the changing magnitude of the brick corrosion rate was slight. When the fluctuation velocity reached 4 $m \cdot s^{-1}$, the corrosion rate of refractory bricks only increased by 0.012 $mm \cdot (100\ h)^{-1}$. Therefore, the gas velocity was not the main control factor for the brick corrosion process. In order to study the effecting mechanism of gas velocity fluctuation, it was assumed that the shear forces on both sides of the gas-slag interface were approximately equal according to the momentum conversation, as shown in the following equations:

$$\tau_g = \tau_s \tag{12}$$

$$-\eta_g \frac{du_g}{dx} = -\eta_s \frac{du_s}{dx} \tag{13}$$

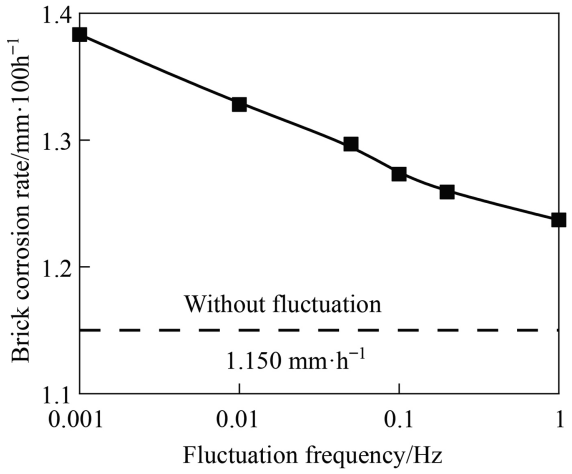

Fig. 9. The influence of the gas fluctuation frequency on the brick corrosion rate.

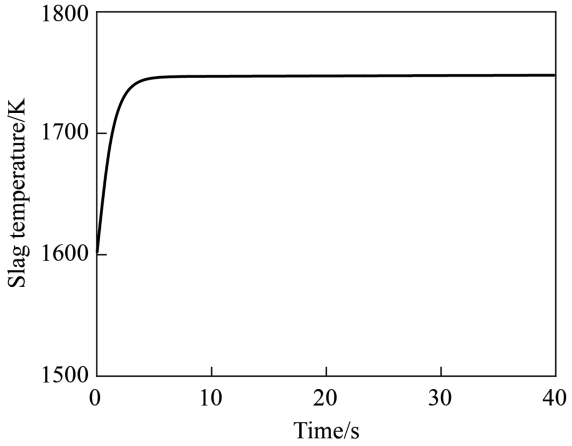

Fig. 10. Characteristic response time of molten slag.

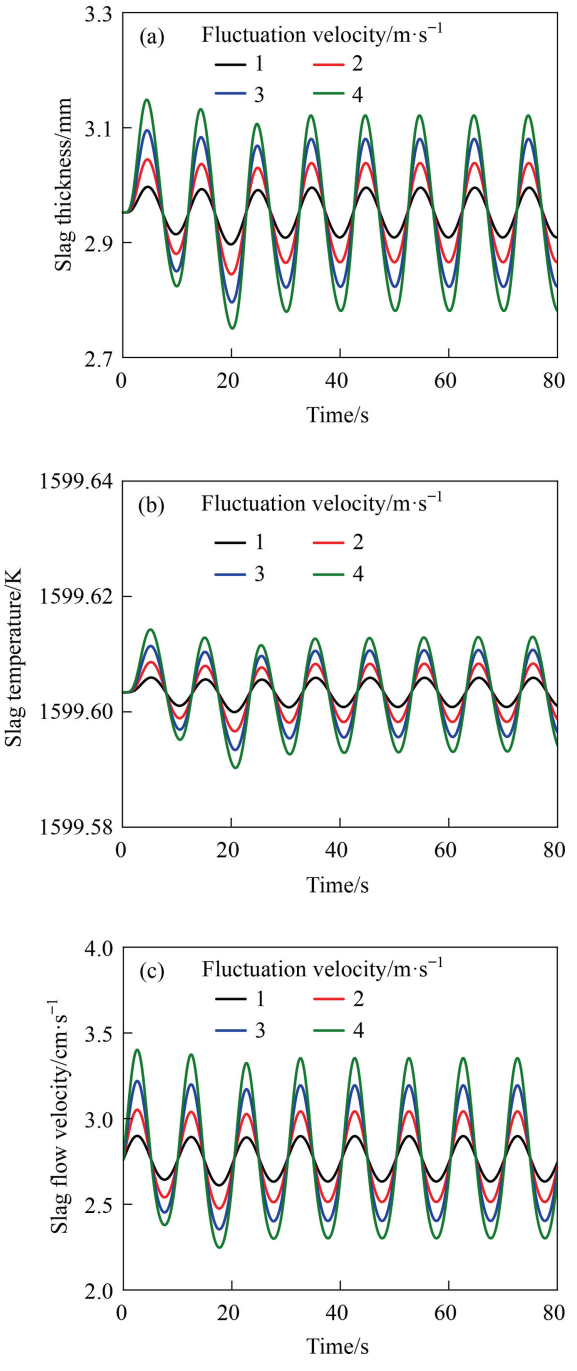

Fig. 11. The influence of the gas velocity fluctuation on (a) slag thickness, (b) slag temperature and (c) slag velocity.

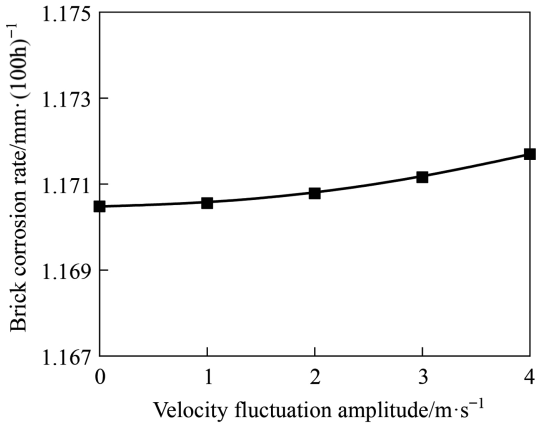

Fig. 12. The influence of the gas velocity fluctuation on brick corrosion rate.

The viscosity of the gas inside the furnace was about 1.72×10^{-5} Pa·s according to the CFD simulation, and the slag viscosity was 8–20 Pa·s. Because of the large viscosity difference between slag and gas, the change of gas velocity had little effect on slag flow behavior.

4.2.3. Gas temperature fluctuation amplitude

Fig. 13 shows the effect of gas temperature fluctuation on slag flow characteristics. In this section, the gas mean temperature and velocity were still 1600 K, and 9 m·s^{-1}, respectively. And the fluctuation frequency was 0.1 Hz. Compared with the fluctuation of gas velocity, the fluctuation of gas temperature had a significant effect on the slag flow characteristics. With the increase of the gas temperature fluctuation amplitude, the changing magnitude of the slag thickness, temperature and flow velocity all increased greatly. The temperature and flow velocity of the slag showed a periodic sinusoidal change with the gas temperature. However, the distributions of the slag thickness were irregular, which were caused by the exponential relationship between the viscosity of the slag and the temperature (Fig. 2). Therefore, the greater the fluctuation of gas temperature was, the more obvious this trend was.

Fig. 14(a) shows the effect of gas-phase temperature fluctuation on the corrosion rate of refractory bricks. The corrosion rate of refractory bricks increased exponentially with the increase of gas temperature fluctuation amplitude. Under the same temperature fluctuation amplitude, the corrosion rate of refractory bricks gradually increased with the decrease of frequency. When the temperature fluctuation amplitude reached 200 K and the fluctuation frequencies were 0.001, 0.01, 0.1, and 1 Hz, the corrosion rates of refractory bricks were 1.57, 1.46, 1.36 and 1.30 mm·(100 h)$^{-1}$, respectively. Besides, in order to reflect the effect of the temperature fluctuation more intuitively, the dimensionless amplitude of brick corrosion rate was defined as j and it could be expressed as follows:

$$j = \frac{J_t - J}{J} \tag{14}$$

where J was the brick corrosion rate without fluctuation, J_t was the brick corrosion rate with fluctuation. Fig. 14(b) shows the evolution of the dimensionless amplitude of brick corrosion rate under different fluctuation temperatures and frequencies. As the fluctuating temperature increased, the dimensionless amplitude of the corrosion rate of refractory bricks gradually increased. When the fluctuation frequency was 0.001 Hz and the gas fluctuation temperature was 200 K, the corrosion rate of refractory bricks increased by 36%.

In order to further study the influence of gas temperature fluctuation on the brick corrosion process, the influence of the change

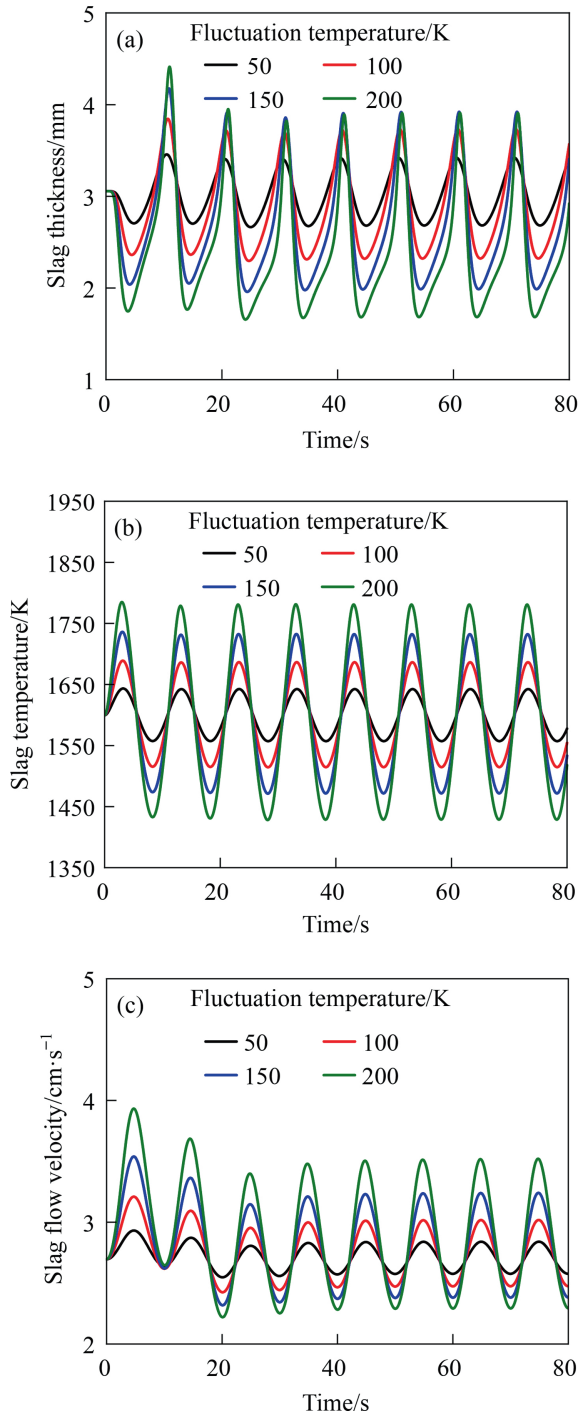

Fig. 13. The influences of the gas temperature fluctuation on (a) slag thickness, (b) slag temperature and (c) slag velocity.

of gas mean temperature on the corrosion rate of refractory brick was studied under the condition that gas temperature fluctuation was 150 K, as shown in Fig. 15. As the gas mean temperature increased, the promotion of the gas temperature fluctuation to corrosion rate of refractory bricks gradually was enhanced. On the one hand, under the condition of high temperature, the influence of gas temperature fluctuation on the service life of refractory brick was more significant. On the other hand, with the change of high-frequency fluctuation to low-frequency fluctuation, the period of fluctuation becomes was prolonged. Therefore, the corrosion rate of refractory brick increased by approximately 20%, 15%, 10% and

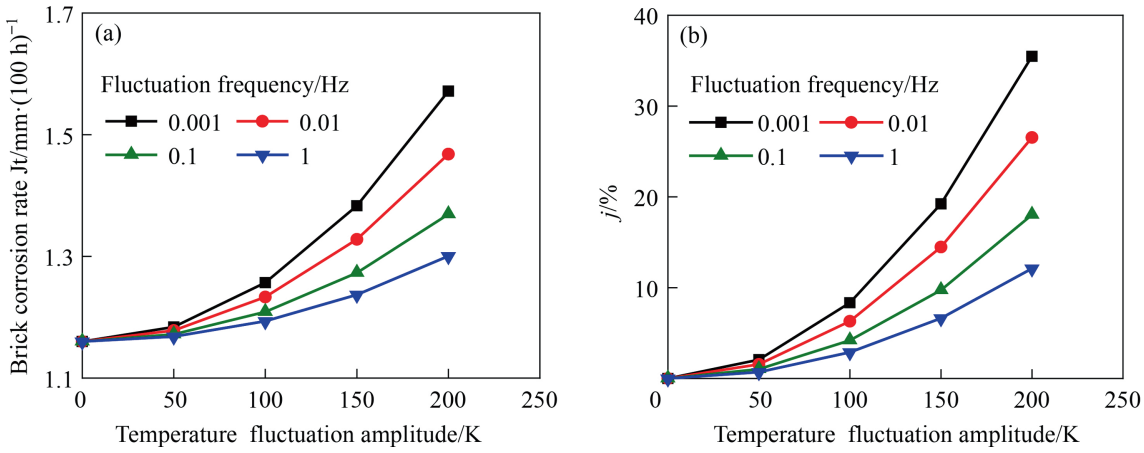

Fig. 14. The evolutions of (a) absolute value and (b) dimensionless value of brick corrosion rate with different gas temperature fluctuation amplitudes and frequencies.

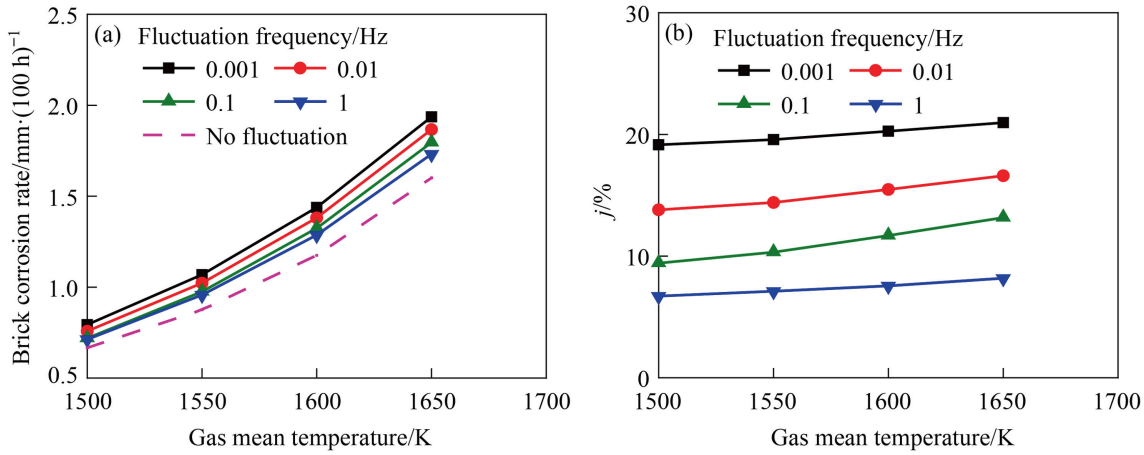

Fig. 15. The influence of the gas mean temperature on (a) absolute value and (b) dimensionless value of brick corrosion rate with the constant temperature fluctuation amplitude.

Table 3
The comparison between the simulation data and industry data

Area	Brick corrosion rate/mm·(100 h)$^{-1}$			Relative error/%	
	Without fluctuation	With fluctuation	Industry data	Without fluctuation	With fluctuation
A	0.700	0.811	0.800	12.509	1.349
B	0.780	0.902	0.940	17.064	4.074
C	1.022	1.204	1.230	16.907	2.135

6% when the fluctuation frequencies were 0.001 Hz, 0.01 Hz, 0.1 Hz and 1 Hz, respectively. Besides, the influence of the gas mean temperature on the dimensionless amplitude of corrosion rate was much less than that of the corrosion rate. The dimensionless corrosion rate increased slightly with the increase of average temperature.

4.3. The comparison of industry data and simulation data

In order to validate the effect of the gas-phase fluctuation, the corrosion rates of refractory bricks in the slag tapping hole of the commercial gasifier (A, B and C areas in Fig. 1) were studied. The characteristic fluctuation temperature and frequency were obtained by the gas temperature fluctuation model, which were 230 K and 0.98 Hz respectively. The industrial data of brick corrosion rate came from a commercial gasifier of plant, which was located at Dalad Banner, Inner Mongolia, China. The brick corrosion rate was obtained by the ratio of brick reduced thickness to operation period. The brick corrosion rates of the A, B and C areas in the lower cone and slag tapping hole under the condition of gas fluctuation were summarized in Table 3. The relative error between the corrosion rates under the condition of fluctuation and no fluctuation with the industry data was defined as:

$$\kappa_r = \frac{J - J_{ind}}{J_{ind}} \times 100\% \tag{15}$$

It was found that the corrosion rate of refractory brick with gas-phase temperature fluctuation increased greatly. Under the condition of the gas fluctuation, the corrosion rate was in good agreement with the industry data, the relative error decreased from 12%−17% to 1%−4%. And it could be concluded that the fluctuation of gas-phase was one of the main reasons for the high corrosion rate of refractory brick at slag tapping hole in the entrained-flow gasifier.

5. Conclusions

A dynamic response model has been adopted to study the slag flow and heat transfer characteristics in a refractory brick lining entrained-flow gasifier. The influences of the gas temperature and flow velocity fluctuation on refractory brick corrosion were investigated. The results showed that the corrosion rate of refractory bricks increased exponentially with the increase of gas-phase temperature in the steady-state. Besides, the gas fluctuation frequencies affected the corrosion rate of refractory brick significantly. When the low-frequency fluctuation changed to the high-frequency fluctuation, the slag characteristic fluctuation amplitude decreased gradually. The slag flow characteristics approximately showed a slight sinusoidal fluctuation with the fluctuation of gas velocity. The gas velocity fluctuation nearly had no effect on the corrosion rate of refractory bricks. And when the gas mean temperature was constant, the characteristic amplitude of the slag flow increased with the increase of the gas fluctuation temperature. Compared with the velocity fluctuation of the gas phase, the temperature fluctuation of the gas phase had a great influence on the corrosion rate of refractory bricks. The fluctuation of gas-phase temperature was the main cause for the low service life of refractory bricks in the tapping hole.

Declaration of Competing Interest

The authors declare that they have no known competing financial interests or personal relationships that could have appeared to influence the work reported in this paper.

Acknowledgements

This work was supported by the National Key Research and Development Program of China (2018YFB0605000).

Nomenclature

A	area of unit, m^2
C	constant in shear force model
C_D	threshold denoted in vortex flame model
C_f	constant in brick corrosion model
C_h	prefactor in vortex flame model
D	furnace inner diameter, m
D_{out}	slag tapping hole diameter, m
d	local diameter, m
f	fluctuation frequency, Hz
h_{sys}	total heat transfer coefficient, $W·m^{-2}·K^{-1}$
J	birck corrosion rate, $mm·(100\ h)^{-1}$
j	dimensionless amplitude of corrosion rate
L	length of the control volume, m
m_{ex}	slag mass outflow rate per unit, $kg·s^{-1}$
m_{in}	mass flow rate of depositing particle, $kg·s^{-1}$
Q_{ex}	heat transfer rate to next unit, W
Q_{in}	heat transfer rate from gas, W
Q_{sr}	heat transfer rate from slag to brick, W
r^*	density ratio
T_g	gas temperature, K
T_s	slag temperature, K
T_{sys}	quenching syngas temperature, K
u	molten slag flow velocity, $m·s^{-1}$
σ	Stefan-Boltzmann constant
β	lean angle
τ	gas-flow shear force
ε_θ	slag emissivity
δ_s	liquid slag thickness, m
δ_m	metal wall thickness, m
δ_{r1}	working brick thickness, m,
δ_{r2}	dense castable refractory thickness, m
ρ_s	slag density, $kg·m^{-3}$
ρ_g	gas density, $kg·m^{-3}$
ρ_{r1}	working brick density, $kg·m^{-3}$
ρ_{r2}	dense castable refractory density, $kg·m^{-3}$
ρ_m	meat wall density, $kg·m^{-3}$
η_s	slag viscosity, Pa·s
λ	thermal conductivity, $W·m^{-1}·K^{-1}$

References

[1] BP, Statistical Review of World Energy, https://www.bp.com/en/global/corporate/energy-economics/statistical-review-of-world-energy/coal.html (accessed in 17 January 2021).
[2] W.D. Wang, D.H. Liu, Y.N. Tu, L.Z. Jin, H. Wang, Enrichment of residual carbon in entrained-flow gasification coal fine slag by ultrasonic flotation, *Fuel* 278 (2020) 118195.
[3] M. Liu, Z. Shen, Q. Liang, J. Xu, H. Liu, Characteristics of single petcoke particle during the gasification process at high temperatures, *Chin. J. Chem. Eng.* 27 (10) (2019) 2427–2437.
[4] Z. Huang, P. Zhang, Y. Yang, J. Sun, J. Wang, Y. Yang, C. Huang, Z. Huang, Acoustic emission detection of slag performance in coal gasifiers, *Chin. J. Chem. Eng.* 28 (8) (2020) 2200–2207.
[5] Z. Dai, X. Gong, X. Guo, H. Liu, F. Wang, Z. Yu, Pilot-trial and modeling of a new type of pressurized entrained-flow pulverized coal gasification technology, *Fuel* 87 (10-11) (2008) 2304–2313.
[6] J. Xu, Q. Liang, Z. Dai, X. Guo, H. Liu, X. Gong, Robust online temperature estimation of a membrane-wall gasifier, *Chin. J. Chem. Eng.* 28 (2) (2020) 556–565.
[7] K. Lin, Z.J. Shen, Q.F. Liang, J.L. Xu, H.F. Liu, Modelling study of characteristics of heat transfer and structural optimization of refractory layer in an entrained-flow gasifier, *Appl. Therm. Eng.* 168 (2020) 114830.
[8] C. He, J. Bai, L.-X. Kong, S. Guhl, D.H. Schwitalla, J. Xu, Z.-Q. Bai, W. Li, The precipitation of metallic iron from coal ash slag in the entrained flow coal gasifier: By thermodynamic calculation, *Fuel Process. Technol.* 162 (2017) 98–104.
[9] C.Y. Li, Cause analysis of the erosion of firebricks in the opposed four-burner gasifier and its improvement, *Coal Chem. Ind.* 41 (1) (2013) 55–57.
[10] P. Biedenkopf, T. Karwath, D. Kobertz, M. Rane, E. Wessel, K. Hilpert, L. Singheiser, Vaporization and corrosion of refractories in the presence of pressurized pulverized coal combustion slag, *J. Am. Ceram. Soc.* 84 (7) (2004) 1445–1452.
[11] M.K. Mahapatra, Review of corrosion of refractory in gaseous environment, *Int. J. Appl. Ceram. Technol.* 17 (2) (2020) 606–615.
[12] M. Müller, K. Hilpert, L. Singheiser, Corrosion behaviour of chromium-free ceramics for liquid slag removal in Pressurized Pulverized Coal Combustion, *J. Eur. Ceram. Soc.* 29 (13) (2009) 2721–2726.
[13] M. Reinmöller, M. Klinger, E. Thieme, B. Meyer, Analysis and prediction of slag-induced corrosion of chromium oxide-free refractory materials during fusion of coal and biomass ash under simulated gasification conditions, *Fuel Process. Technol.* 149 (2016) 218–230.
[14] T.K. Kaneko, H. Thomas, J.P. Bennett, S. Sridhar, M. Rigaud, Synthetic coal slag infiltration into varying refractory materials, *J. Am. Ceram. Soc.* 95 (10) (2012) 3325–3333.
[15] C.W. Andrés, M.N. Moliné, S. Camelli, A.G. Tomba Martinez, Slag corrosion of alumina-magnesia-carbon refractory bricks by different approaches, *Ceram. Int.* 46 (15) (2020) 24495–24503.
[16] S.X. Zhao, B.L. Cai, H.G. Sun, P.T. Li, S.Z. Yan, G. Shi, G. Wang, Thermodynamics simulation on corrosion of high chrome bricks by gasifier slags, *Refractories* 49 (1) (2015) 13–16.
[17] D. Bi, Q. Guan, W. Xuan, J. Zhang, Numerical simulation of GSP gasifier under different swirl angles, *Fuel* 155 (2015) 155–163.
[18] X. Wu, T. Li, J. Cai, Z. Peng, Z. Yuan, Numerical prediction of particle number concentration distribution in scrubbing-cooling chamber of entrained-flow coal gasifier, *Chem. Eng. J.* 149 (1-3) (2009) 325–333.
[19] M. Troiano, F. Montagnaro, R. Solimene, P. Salatino, Modelling entrained-flow slagging gasification of solid fuels with near-wall particle segregation, *Chem. Eng. J.* 377 (2019) 119962.

[20] I. Ye, C. Ryu, Numerical modeling of slag flow and heat transfer on the wall of an entrained coal gasifier, *Fuel* 150 (2015) 64–74.
[21] H.-H. Lee, J.-C. Lee, Y.-J. Joo, M. Oh, C.-H. Lee, Dynamic modeling of Shell entrained flow gasifier in an integrated gasification combined cycle process, *Appl. Energy* 131 (2014) 425–440.
[22] M. Seggiani, Modelling and simulation of time varying slag flow in a Prenflo entrained-flow gasifier, *Fuel* 77 (14) (1998) 1611–1621.
[23] K. Lin, Z.J. Shen, Q.F. Liang, J.L. Xu, H.F. Liu, Modelling of slag flow and prediction of corrosion state of refractory bricks in an entrained-flow gasifier, *Fuel* 275 (2020) 117979.
[24] K. Lin, Z.J. Shen, Q.F. Liang, J.L. Xu, X.L. Guo, H.F. Liu, The effect of the shear force applied by gas-flow in furnace on slag flow characteristics and gasifier performance, *Fuel Process. Technol.* 216 (2021) 106794.
[25] M. Tsue, T. Kadota, M. Kono, Temperature and velocity fluctuations of a jet diffusion flame in a cross-flow, *Proc. Combust. Inst.* 29 (2) (2002) 1937–1942.
[26] B. Zhang, Z. Shen, Q. Liang, J. Xu, H. Liu, Numerical study of dynamic response analysis of slag behaviors in an entrained flow gasifier, *Fuel* 234 (2018) 1071–1080.
[27] K. Lin, Z.J. Shen, Q.F. Liang, J.L. Xu, X.L. Guo, H.F. Liu, The study of slag discharge behavior of entrained-flow gasifier based on the viscosity-temperature characteristics of different types of coals, *Fuel* 292 (2021) 120314.
[28] J. Xu, Q. Liang, Z. Dai, H. Liu, Comprehensive model with time limited wall reaction for entrained flow gasifier, *Fuel* 184 (2016) 118–127.
[29] B. Zhang, Z. Shen, Q. Liang, J. Xu, H. Liu, Modeling study of residence time of molten slag on the wall in an entrained flow gasifier, *Fuel* 212 (2018) 437–447.
[30] D. Shaw, R. Essenhigh, Temperature fluctuations in pulverized coal (P.C.) flames, *Combust. Flame* 86 (4) (1991) 333–346.
[31] Y. Gong, Q. Guo, J. Zhang, P. Fan, Q. Liang, G. Yu, Impinging flame characteristics in an opposed multiburner gasifier, *Ind. Eng. Chem. Res.* 52 (8) (2013) 3007–3018.
[32] J. Xing, Y. Bai, C. Zhao, Z. Gao, H. Wang, Numerical studies of coal devolatilization characteristics with gas temperature fluctuation, *Energy Fuels* 32 (8) (2018) 8760–8767.
[33] X. Xia, P. Zhang, A vortex-dynamical scaling theory for flickering buoyant diffusion flames, *J. Fluid Mech.* 855 (2018) 1156–1169.
[34] P. Lian, A.o. Huang, H. Gu, L. Fu, S. Wang, Corrosion mechanism of foamed slag on the lightweight corundum-spinel castable, *Interceram. – Int. Ceram. Rev.* 65 (6-7) (2016) 226–231.
[35] M. Nath, S. Song, Y. Li, Y. Xu, Effect of Cr_2O_3 addition on corrosion mechanism of refractory castables for waste melting furnaces and concurrent formation of hexavalent chromium, *Ceram. Int.* 44 (2) (2018) 2383–2389.
[36] K. Kwong, A. Petty, J. Bennett, R. Krabbe, H. Thomas, Wear mechanisms of chromia refractories in slagging gasifiers, *Int. J. Appl. Ceram. Technol.* 4 (6) (2007) 503–513.
[37] J. Matyas, S.K. Sundaram, B.J. Hicks, A.B. Edmondson, B.M. Arrigoni, Slag-refractory interaction in slagging coal gasifiers, *Mater. Sci. Forum* 595-598 (2008) 397–405.
[38] J. Xu, Z. Dai, H. Liu, L. Guo, F. Sun, Modeling of multiphase reaction and slag flow in single-burner coal water slurry gasifier, *Chem. Eng. Sci.* 162 (2017) 41–52.
[39] A. Silaen, T. Wang, Effect of turbulence and devolatilization models on coal gasification simulation in an entrained-flow gasifier, *Int. J. Heat Mass Transf.* 53 (9-10) (2010) 2074–2091.